In Vivo Characterization of a Wireless Telemetry Module for a Capsule Endoscopy System Utilizing a Conformal Antenna

Julia Faerber, *Student Member, IEEE*, Gerard Cummins, *Member, IEEE*, Sumanth Kumar Pavuluri, Paul Record, Adrian R. Ayastuy Rodriguez, Holly S. Lay, Rachael McPhillips, Benjamin F. Cox, Ciaran Connor, Rachael Gregson, Richard Eddie Clutton, Sadeque Reza Khan, Sandy Cochran, and Marc P. Y. Desmulliez, *Senior Member, IEEE*

***Abstract*—This paper describes the design, fabrication, packaging, and performance characterization of a conformal helix antenna created on the outside of a 10 mm × 30 mm capsule endoscope designed to operate at a carrier frequency of 433 MHz within human tissue. Wireless data transfer was established between the integrated capsule system and an external receiver. The telemetry system was tested within a tissue phantom and *in vivo* porcine models. Two different types of transmission modes were tested. The first mode, replicating normal operating conditions, used data packets at a steady power level of 0 dBm, while the capsule was being withdrawn at a steady rate from the small intestine. The second mode, replicating the worst-case clinical scenario of capsule retention within the small bowel, sent data with stepwise increasing power levels of –10, 0, 6, and 10 dBm, with the capsule fixed in position. The temperature of the tissue surrounding the external antenna was monitored at all times using thermistors embedded within the capsule shell to observe potential safety issues. The recorded data showed, for both modes of operation, a low error transmission of 10^{-3} packet error rate and 10^{-5} bit error rate and no temperature increase of the tissue according to IEEE standards.**

***Index Terms*—Capsule endoscopy, conformal antenna, helix antenna, ingestible medical devices, implantable devices, *in vivo* data transmission, wireless capsule endoscopy, wireless data transmission.**

Manuscript received June 13, 2017; revised August 14, 2017; accepted September 24, 2017. Date of publication November 3, 2017; date of current version January 26, 2018. This work was supported by the U.K. Engineering and Physical Sciences Research Council through the Program Grant entitled "Sonopill: minimally invasive gastrointestinal diagnosis and therapy" under Grant EP/K034537/1 and Grant EP/K034537/2. This paper was recommended by Associate Editor H. Jiang. *(Corresponding author: Julia Faerber.)*

J. Faerber, G. Cummins, S. K. Pavaluri, P. Record, A. R. A. Rodriguez, S. R. Khan, and M. P. Y. Desmulliez are with the Institute of Sensors, Signals and Systems, School of Engineering and Physical Sciences, Heriot-Watt University, Edinburgh EH14 4AS, U.K (e-mail: jf141@hw.ac.uk; G.Cummins@hw.ac.uk; Sumanth_Kumar.Pavuluri@hw.ac.uk; P.Record@hw.ac.uk; ara4@hw.ac.uk; srk5@hw.ac.uk; M.Desmulliez@hw.ac.uk).

H. Lay, R. McPhillips, C. Connor, and S. Cochran are with the School of Engineering, University of Glasgow, Glasgow G12 8QQ, U.K (e-mail: Holly.Lay@glasgow.ac.uk; Rachael.McPhillips@glasgow.ac.uk; 2029831C@student.gla.ac.uk; sandy.cochran@glasgow.ac.uk).

B. F. Cox is with the School of Medicine, University of Dundee, Dundee DD1 4HN, U.K (e-mail: b.cox@dundee.ac.uk).

R. Gregson and R. E. Clutton are with the Wellcome Trust Critical Care Laboratory for Large Animals, Roslin Institute, Midlothian EH25 9RG, U.K (e-mail: Rachael.Gregson@ed.ac.uk; E.Clutton@ed.ac.uk).

Color versions of one or more of the figures in this paper are available online at http://ieeexplore.ieee.org.

Digital Object Identifier 10.1109/TBCAS.2017.2759254

Fig. 1. Configuration of Pillcam SB with internal helix antenna [1].

I. Introduction

WIRELESS capsule endoscopy (WCE) is an accepted diagnostic modality for imaging the gastrointestinal tract (GI) complimenting conventional endoscopy. The small size of these capsules (typically 11 mm diameter, 26 to 31.5 mm length) makes them easy to swallow and allows access to the small bowel, which is difficult to reach using conventional endoscopy. Their size has consequently led to greater patient acceptance, which is beneficial for improved diagnosis and management of gastrointestinal disorders.

WCE became commercially available in 2001 and, since then, have predominantly relied on optical imaging modalities [2]. Various other sensing modalities have been suggested over the years to increase their diagnostic potential [3], [4]. One modality being investigated by the Sonopill project [5] is the use of combined ultrasound (US) and optical imaging to improve the early diagnosis of a wide variety of gastrointestinal disorders, such as Crohn's disease or colorectal cancer, as US enables the detection of subsurface neoplasms amongst other pathologies [3], [5], [6].

However, denser integration due to an increased number of modalities within the capsule leads to increasing challenges due to the limited space available within the capsule. This makes it more difficult for relatively larger components such as a typical internal helix antenna to fit within the capsule without a reduction in sensing capabilities, as shown in Fig. 1.

Previously designed conformal antennas cover either most of the capsule surface, represent larger dimensions due to the larger size of the capsule or radiate at higher frequencies [7]–[13]. Liu *et al.* and Das *et al.* present conformal antennas radiating at 2.4 GHz and 915 MHz and demonstrated their performance in

simple body models, composed of a liquid mixture and minced pork respectively [10], [12]. None of the state of the art conformal ingestible antennas has yet been investigated completely in vivo together with a data transmission chip and temperature/SAR measurements. In the following we demonstrate the design, manufacturing and performance characterisation of a helical antenna conformally placed outside an endoscopic capsule and the characterisation in silico, in vitro and in vivo of the telemetry system in porcine models. This method does not utilize the internal volume of the capsule, but requires additional coating to protect the antenna from the surrounding tissue and maintain biocompatibility [14], [15].

Utilizing the external surface of the shell also allows an effective increase in antenna size. The resulting increased antenna length allows operation at a lower resonance frequency in the MHz range offering higher radiation efficiency within high dielectric materials such as human body tissue. Ingestible antennas radiate at frequencies in the GHz range in free space. When inserted into high-permittivity dielectric body materials their effective wavelength is shortened. The resulting lower resonance frequency compared to air makes the antenna less susceptible to signal attenuation [16]–[18]. The antenna performance is strongly affected by the surrounding tissue, reducing its radiation efficiency, changing the radiation distribution and input impedance. The interaction of microwaves with biological materials is described in detail by Vander Vorst *et al.* [19] and more information about dielectric properties of human tissues can be found in Gabriel *et al.* [20]–[22]. To evaluate the effects of human body tissue on the wave attenuation, the theoretical path loss model for both male and female human phantom has been presented in [23] and it has been reported that at 402.5 MHz and for the dipole antenna the far field begins at a distance of 47.5 mm from the source. In addition the high dielectric insulation layer, considered as part of the emitter antenna system, lowers the attenuation of electromagnetic fields through the body layers [15].

The antenna should have sufficient bandwidth to transmit the sensor data within a reasonable time frame to an external receiver. The typical frame rate of these devices is around 2 to 6 frames per second (fps), although many new devices, such as the PillCam COLON2, operate at 35 fps due to the use of video compression and adaptive frame rate techniques [24]–[27]. The frame size itself varies from 256 $\times$ 256 pixels up to 1,920 $\times$ 1,080 pixels comprised of 192 kB to 3,000 kB with 8 bit RGB color depth depending on the imaging camera used [25], [28]–[30].

In this paper, we present the design, simulation, manufacturing and characterization of a transceiver system using a conformal helix antenna on a prototyped endoscopic capsule shell with integrated electronics. This integrated system has been successfully tested using human tissue phantoms and *in vivo* porcine models. The prototype development is described in Section II and includes design and simulation of the antenna, electronic design and assembly as well as construction of the capsule and antenna. Section III describes the experimental setup for the phantom measurements as well as the *in vivo* porcine trials. Results of both trials (phantom, animal) are provided in Section IV and discussed in Section V. Final conclusions are given in Section VI.

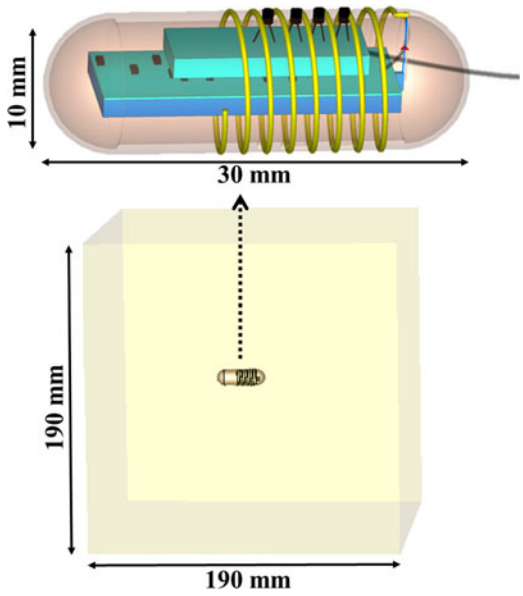

Fig. 2. Simulation setup of the helix antenna system within a cubic muscle tissue model.

II. Prototype Development

A. Antenna Design and Simulation

A helix shaped antenna was modelled and its characteristics were simulated to assess its performance within a human body tissue environment. This design allows the extension of the electrical length of the conductive copper wire while ensuring that the occupied external surface area of the capsule stays small [31]. The helix shape was selected as previous studies have shown that the helix is less likely to be detuned in different dielectric body tissues [31]. Such an antenna can be easily integrated along the pill curvature while maintaining the antenna geometry and can be designed at the required operating frequency of 433 MHz. This frequency is part of the ISM band (Industry, Science and Medical) and is commonly used in commercially available short range transceiver modules. The antenna has a wide bandwidth of 20 MHz, which is consistent over a variety of tissue types [32].

The maximum size of 10 $\times$ 30 mm of the Sonopill was chosen to be able to incorporate the batteries, camera, LEDs and the US array. The domes will be used by the camera at one end and the US array electronics on the other side. Therefore the antenna was designed to cover the length of the capsule as a proof of concept. Different designs can be incorporated at a later stage.

Fig. 2 shows the simulation setup of the proposed antenna. The antenna was simulated within a homogeneous cubic tissue phantom model, large enough to ensure the electromagnetic energy is completely absorbed (190 $\times$ 190 $\times$ 190 mm^3). The cubic shape offers a reduction of computational resources and the simulated phantom material matches the purchased body phantom material with muscle equivalent dielectric properties

(real permittivity $\varepsilon_r = 62$, loss tangent $\tan\delta = 0.7$). Muscle tissue was used, as it causes a larger signal attenuation due to its high permittivity ($\varepsilon_r = 65$) at 433 MHz compared to fat ($\varepsilon_r = 5.6$) or bone ($\varepsilon_r = 13.1$). Therefore, it provides a worst case scenario when investigating the antenna radiation properties [33]. All parts of the system, apart from the influence of the attached tether, were considered in the simulation, including the connection of the antenna to the internal ground (GND) plane and the external insulation layer. The dielectric properties of all materials were measured prior to the simulations such that their lossy and frequency dependent dispersive characteristics, which significantly influence the simulation results, can be integrated.

The optimal length of the antenna, determined by the CST Microwave Studio^{TM} simulation software optimization tools, was 7.75 turns for an antenna made of 400 μm diameter copper wire, with a pitch of 1.6 mm and a radius of 4.8 mm. This is equivalent to a helix length and height of 240 mm and 12.5 mm, respectively, occupying thereby less than half of the external capsule surface. Thus, more than half of the capsule area is available for the integration of other modalities such as cameras and sensors necessitating windows to the outside world.

The simulated radiation pattern of the antenna system, including the gain and radiation efficiency, is shown in Fig. 3(a). The simulated antenna has a gain of -40.9 dB, with an almost omnidirectional radiation pattern, and a low efficiency of -41.2 dB, which is due to the absorption of electromagnetic waves in the human body [34].

Fig. 3(b) shows the comparison between the simulated resonance frequencies of the full antenna system with connected and disconnected GND plane, and the measured resonant frequency of the fabricated prototype within the phantom using a programmable network analyzer (PNA N5225A) (Agilent, USA). The GND plane is placed longitudinally inside the shell. In the assembled device, the antenna is connected to the center pin of the micro-SMA connector mounted on the PCB and the GND is connected to the outer shield of the SMA. The antenna, when measured, was not connected to the assembled PCB system as it was not possible to attach the PNA cable to the RF board. The simulated resonance frequency of the full system shows that the resonance frequency lies within the targeted ISM band at 433 MHz with a bandwidth of 20 MHz. This wide bandwidth characteristic helps to maintain a reflection coefficient below -10 dB while the capsule is travelling through different body tissues. When the GND in the simulation is disconnected, the frequency shifts down by 20 MHz. The measured device disconnected from the GND plane shows a shift of 20 MHz to a higher frequency. The difference in the S_{11} response between the simulated and measured results can be primarily attributed to two effects. In order to measure the response of the antenna, an additional SMA connector and a short coaxial cable (2 cm) have been added for obtaining the measurements from the PNA. The parasitics of the coaxial cable and the SMA could have contributed for the shift in the resonance frequency. This effect has also been noticed in a similar study in [35]. In addition the measurements with the PNA have been performed with the ground plane of the helix removed. It is known that the transmission and

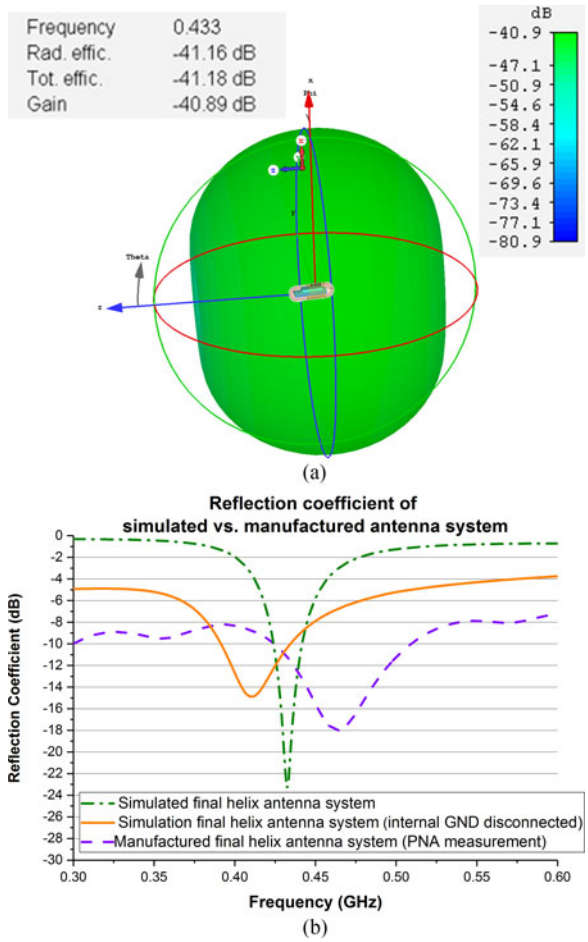

Fig. 3. (a) Radiation pattern of the antenna system with gain and radiation efficiency value. (b) Resonance frequency of the simulation of the full antenna system with connected and disconnected GND plane and the fabricated prototype measured within the phantom with a PNA.

radiation modes of a helix antenna can vary depending on the geometry of the helix and these effective geometry parameters in turn depend on the effective dielectric properties of the phantom material. The effective dielectric properties of the tissues have been known to change depending on the condition of the porcine [36]. The coaxial cable geometry along with the helix could have contributed for the occurrence of combination of transmission and radiation modes, thereby increasing the measured effective bandwidth of the helix antenna. Differences between the simulation in terms of resonance frequency and bandwidth are due to the disconnection of the GND plane for our measurements. Due to the lack of GND plane connection, an offset of the reflection coefficient (<0 dB) is visible. In this case most of the power was not radiated, but returned to the antenna system.

Thermal transfer measurements were used as an indication of the Specific Absorption Rate (SAR) which should not exceed 1.6 W/kg for 10 grams of tissue mass [37], [38]. SAR is a measure of the rate at which energy is absorbed by the tissue when exposed to a RF electromagnetic field. Interaction of electromagnetic fields with biological tissue at MHz frequencies can cause thermal effects, due to the absorption of energy

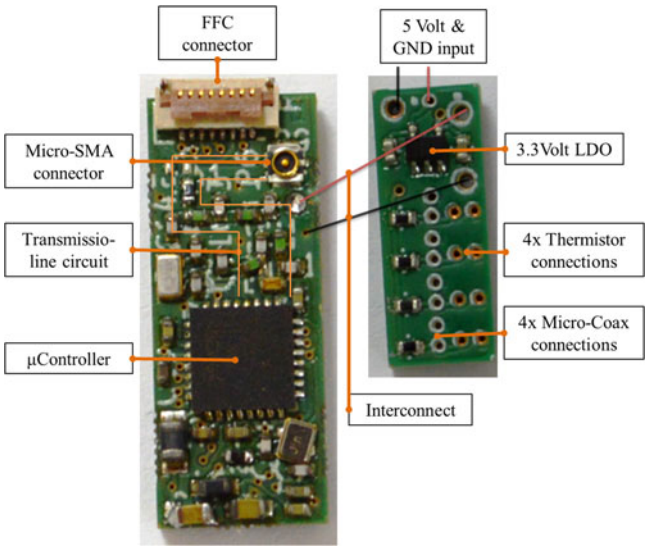

Fig. 4. (Left) RF board and (right) thermistor board.

within the high dielectric tissue. Electrically small antennas in close proximity of human tissues can be a hazard when excited, therefore embedded thermistors have been used to monitor potential thermal effects. Simulations have also shown that the glass encapsulating the negative temperature coefficient (NTC) thermistors and embedded into the capsule shell did not influence the antenna performance significantly and can therefore be ignored in further simulations.

B. Circuit Design and Prototype Assembly

Six capsule shells of 10 mm diameter and 30 mm length were produced from VeroWhite polymer using the Polyjet additive manufacturing process on a Stratasys Objet500 Connex. The high print resolution of 600 dpi $\times$ 600 dpi ($42 \times 42\,\mu m^2$) in the x-y plane and 16 μm layer thickness along the z-axis direction allows the creation of grooves along the external surface of the capsule to be reliably shaped into the desired antenna geometry. The internal diameter of the capsule was 8.5 mm in order to accommodate the printed circuit boards (PCBs) shown in Fig. 4, that contain the electronic system for operating the antenna.

Two PCBs per capsule were designed. The RF board contains ($8.29 \times 21 \times 1.54\,mm^3$) the antenna connection, matching network and programmable microcontroller unit (MCU). The thermistor board ($5.3 \times 13.8 \times 1.54\,mm^3$) comprises the low dropout voltage regulator (LDO), thermistor circuit connections and power supply. Four thermistors were embedded into the capsule shell, to allow the measurement of any temperature rise in the surrounding tissue near the antenna as traditional SAR measurements in proximity of the antenna were not possible during the *in vivo* trials.

The MCU chosen to control the system was an ARM Cortex-M3 based wireless microcontroller combined with an ultra-low power RF transceiver (CC1310, Texas Instruments (TI), USA), as it supports the required frequency bands and comes in small size packages ($5 \times 5\,mm^2$).

The MCU provides 32 pins out of which 15 are general purpose input/output (GPIO) pins with two unbalanced output pins leading to the transmission line circuit consisting of a 50 Ω impedance matching circuit. The main components and connections include the JTAG connection that was used to transfer the program from the Code Composer Studio (CCS) provided by TI to the MCU, a 24 MHz and a 32 kHz crystal oscillator (Murata, JPN and AVX, USA) and finally the transmission line circuit. The thermistor board contained 4 NTC thermistors (B57540G1 from TDK Group) in individual voltage divider circuits, as well as a LDO (ON Semiconductor, USA), which converted the 5 V supplied via the tether to 3.3 V.

The simulation of the final transmission line design, from MCU to micro-SMA, performed with the Advanced Design System (ADS) software showed an impedance of 58 Ω, which was an acceptable result for the antenna to work at the required frequency band.

A 3 mm diameter port was present at one end of the capsule for the attachment of the tether. Due to space limitations and to reduce complexity the temperature data was not transmitted wirelessly but instead via the tether bundle, which was connected to an external data logging system. The use of a 3 m long tether also facilitated retrieval of the capsule after the completion of the *in vivo* studies and enabled power to be transmitted without the need for integrated batteries. The tether consisted of 4, 42 AWG micro-coax cables (AlphaWire, USA) and two, 30 AWG single core cables (AlphaWire, USA), which were inserted into biocompatible Teflon tubing (inner diameter = 3 mm and outer diameter = 4 mm) (Adtech, USA).

The single core-wire was used for power transmission, while the micro-coaxial wire was used for signal transmission. Four micro-coaxial cables were soldered to the thermistor circuit. The thermistors embedded between the antenna tracks along the external surface of the shell were fixed in place using adhesive EP42HT-2Med (Masterbond, USA). One single core wire was soldered to the input of the LDO and another, which acted as a GND cable, was soldered to a GND pad on the thermistor board. The RF board was connected with two pieces of micro-coaxial cables to the thermistor board. One connection linked the output of the LDO to the power input of the MCU and the second cable joined the GND connection. The enameled copper wire antenna (diameter = 0.4 mm) (Block, USA) was soldered to a micro SMA cable (Murata Manufacturing Co., Ltd., JPN) which was then attached to the matching micro SMA connector (type: JSC series).

After PCBs assembly, the two parts of the capsule were aligned and sealed using EP42HT-2Med, an USP Class VI biocompatible epoxy (Master Bond Inc., USA). After curing, the copper wire was threaded along the grooves in the shell to form the antenna. The capsules were then coated to avoid any leaks and to fix the tubing in place, using the same biocompatible epoxy as previously mentioned. In addition, the layer of epoxy helps reducing the SAR and the power absorbed by the body [39].

To guarantee an even distribution of the epoxy over the full length of the capsule, particularly across the antenna, molds were manufactured to produce a uniform 400 μm thick film.

The molds were created by using two additively manufactured forms made of VeroWhite polymer (Stratasys, USA) and filled with a silicone elastomer Sylgard 184 (Dow Corning, USA). The cured flexible molds were sprayed with polymer remover (Ambersil) and the assembled capsules were placed into one part of the cured mold. The second part was manually aligned with the other half and secured with a clamp. To ensure its even coverage, the epoxy was degassed prior to use by placing the filled molds into a bell jar and operating a vacuum pump in 30 seconds on-off cycles until the gas bubbles disappeared. The epoxy was then injected into the mold with a syringe until the cavity was completely filled. The epoxy was cured for 6 hours at 55 °C. Afterwards the mold was removed from the capsule. The epoxy film thickness was measured using a digital caliper to be between 400 and 500 μm. The final step involved the coating of the capsule in a conformal layer of Parylene-C, which is a widely used biocompatible material known for its dry lubricant properties. The reduction of friction between the capsule and the surrounding tissue should ensure ease of insertion and ease of movement along the GI tract.

The two power cables and the four temperature data cables of the tether were soldered to a low-voltage differential signaling (LVDS) connector DF80 (Hirose Electric Co., Ltd, JPN). This connector was attached to a custom-made adapter with an on-off switch. This on-off switch allows immediate termination of the experiment if failure of the capsule is detected or if the surrounding tissue temperature exceeds 40 °C. The adapter allowed communication between the capsules and the myRIO 1900 portable embedded device hardware (National Instruments, USA), which is controlled via USB with a LabVIEW (National Instruments, USA) user interface on the laptop. The myRIO provided a 5 V power supply to the capsule via the tether through the output power pin upon connection to the laptop and the thermistor connections were connected to 4 analog inputs of the myRIO. The entire assembling process is illustrated in Fig. 5.

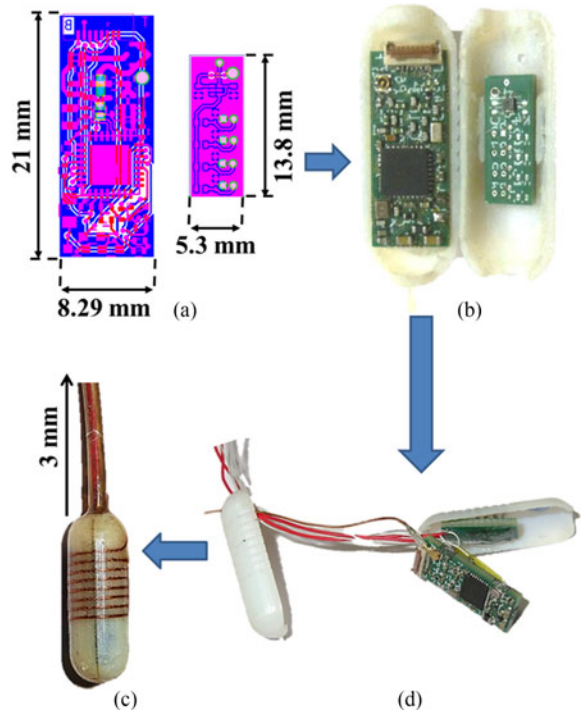

Fig. 5. Design and manufacturing process of the full transceiver system. (a) Designed PCB of RF and thermistor board. (b) Position of the boards inside the capsule. (c) Tether connection. (d) Fully packaged capsule with antenna.

C. Phantom Fabrication

The antenna simulation results were compared with experimental results obtained from testing the capsule within a tissue phantom. Previously, dry and liquid phantoms have been used to mimic different tissue properties [40], [41]. The phantom material used in these tests consists of a hydrophilic organic powder and degassed water (Super stuff bolus, RPD Inc., USA), which was mixed in a weight ratio of 6:1 (powder: water) reproducing thereby the electromagnetic properties of the muscle tissue, as shown in Fig. 6(a). This material can be easily shaped, has a long shelf life of 6–9 months and, by adjusting the mix ratio, different tissue properties can be obtained (e.g., less water used reduces permittivity of material). The doughy consistency of the phantom ensures that electronic equipment does not come into contact with any water, which reduces the risks of a short circuit. Due to its gelatinous nature and low transmission frequency, a coaxial type probe was used to evaluate the frequency dependent complex permittivity and loss tangent of the phantom material. This ensured an accurate measurement over a wide bandwidth. Commercially available probes (e.g., Keysight N1501A dielectric probe kit) are expensive and are often more reliable in measuring liquids and solids than gels. Measurements of the phantoms dielectric properties were conducted at the National Physical Laboratory (NPL), using their custom made coaxial sensor [42]. The measured dielectric properties are shown in Table I.

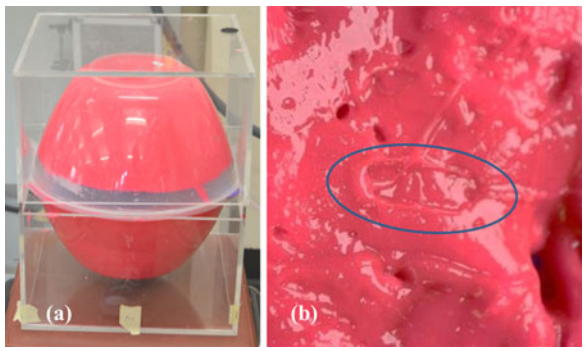

Fig. 6. (a) Entire phantom setup. (b) Indentation of capsule in phantom.

TABLE I
COMPARISON OF DIELECTRIC PROPERTIES AT 433 MHZ

	Simulation	Phantom	Muscle tissue
Relative permittivity ε_r	65.5	65.7	58
Loss tangent tanδ	0.68	0.7	0.84

III. Measurement Setup

This section describes the experimental measurement setup for the proposed data transceiver antenna. Six capsules were fabricated in total and were divided into two groups of three. The MCU of each group of capsules was programmed differently to allow characterization of the antenna under different transmission settings.

A. Transceiver Setup

The antennas of the first group transmitted with a constant output power level of 0 dBm (1 mW) while being manually moved along the small bowel during the porcine tests. The antennas of the second group transmitted at output power levels, while the capsule remained motionless within the small bowel. The transmitted power levels were 0.1, 1, 4 and 10 mW (–10, 0, 6, 10 dBm). The power levels remained constant for 5 minutes and 20 seconds. This time frame corresponds to the duration of submission of 2 frames of 326 kBytes. After this time, the antennas were switched off for 5 minutes, before the power level was set up to the next higher level.

While wireless RF data packets are being transmitted the temperature of the surrounding tissue was being continuously monitored via the embedded thermistors, and the temperature data was sent via the attached tether.

The microcontroller was programmed with Code Composer Studio provided by TI to send data packets composed of a message header, a package counter, a time stamp and the RSSI (Received Signal Strength Indicator). The maximum data payload was 255 bytes per packet. The transceiver (CC1310, TI) offers a wide range of data rates from 625 bps to 4 Mbps and an automatic cyclic redundancy check (CRC). The modulation format used was the GFSK for the carrier frequency of 433 MHz with a deviation of 127 kHz.

The data packets were received by a CC1110 receiver (RX) module (TI, USA) attached to the SmartRF Transceiver Evaluation Board (TrxEB, TI, USA) that was connected via USB to a laptop. The SmartRF Studio firmware (TI, USA) was used to control the receiver parameters and to monitor and collect information about packet error rate (PER) and bit error rate (BER) data. The RX filter bandwidth was set to 541 kHz and the channel spacing to 200 kHz, all other parameters were selected to match those of the transceiver (TX).

B. Phantom Measurements

The capsule antennas were embedded within a molded sphere of 28 cm diameter made of the tissue phantom shown in Fig. 6(a). The capsule was placed within an indented, recessed outline of the capsule within the tissue phantom as shown in Fig. 6(b). This ensured that the position of the capsule within the tissue phantom was fixed for each experiment. The second phantom part was placed on top to evenly surround the capsule with the dielectric material. Once placed, the signal strength (RSSI) over distance as well as the radiation pattern of each capsule antenna was recorded. Measurements over distance and different orientations between the TX and RX were performed to analyze their influences over the signal strength. The capsules were inserted into the phantom with the tether connection pointing vertically upwards. The distance between RX and TX was increased incrementally in 10 cm steps from 20 to 70 cm. The data was recorded for 10 seconds at each step. Additionally, the capsules were inserted horizontally and vertically (tether connection pointing up) into the phantom to observe the effect of capsule orientation on the signal strength. The RX was moved in 45° steps around the TX placed at a distance of 50 cm.

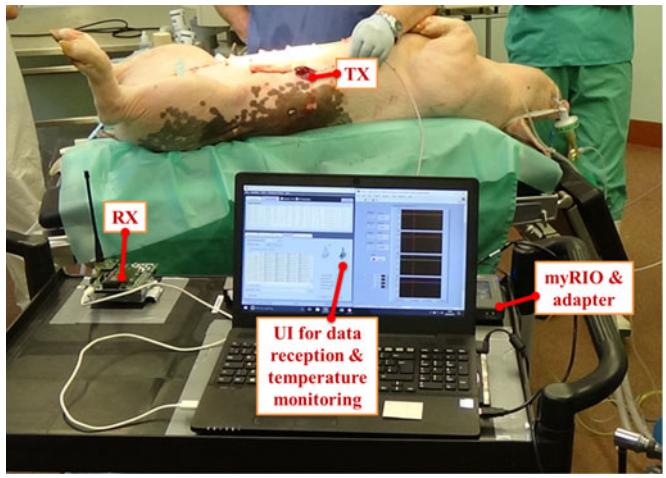

Fig. 7. Porcine trial setup: Capsule (TX) inserted via the created stoma; RX, laptop for data recording and TI adapter placed on trolley next to pig.

C. In Vivo Trials

The performance of the capsule antenna was characterized using *in vivo* porcine models. These tests were conducted in collaboration with the Wellcome Trust Critical Care Laboratory for Large Animals (Roslin Institute, Roslin, UK) under license from the UK Home Office (PPL 70/8812). The age of the pigs ranged from 3 to 4 months and the weight ranged from 56 kg to 64 kg. Anaesthesia was induced with isoflurane ("Isoflo" Zoetis, Surrey), vaporized in oxygen and nitrous oxide administered via a Bain breathing system and face mask. A cannula was placed in the auricular vein and the trachea was intubated. Anaesthesia was maintained with isoflurane. Ringer's lactate solution ("Aquapharm No 11"; Animalcare, North Yorkshire) was administered at 10 ml kg^{-1} h^{-1} throughout the study. The pigs' lungs were mechanically ventilated to maintain normocapnia. Vital signs were monitored throughout the experiment by an experienced veterinary anaesthetist. When the experiments were complete, the animals were euthanised without recovery from anaesthesia using pentobarbital.

The capsules were inserted 60 cm into the small bowel via a stoma. The setup of the experiments is represented in Fig. 7 and summary of the pigs' experimental conditions is given in Table II. Lubrication to facilitate insertion of the capsules was provided by a 0.9% by volume saline drip at the stoma entrance and a thermometer was inserted 60 cm passed this point, which recorded the internal temperature of the small bowel before and after each experiment. Two live pigs (PigX and PigY) were utilized.

TABLE II
PIG EXPERIMENTAL SETUP

	PigX	PigY = PM1
Age (months)	4	5
Weight (kg)	60	70
Distance between stoma and RX (cm)	62	70

An ultrasound system (Siemens Sonoline Antares) was used whenever possible to locate the capsules within the small bowel. The thermistor data was continuously monitored and recorded using a Labview UI.

The experimental system was fixed onto a trolley to facilitate portability between venues. The RF equipment trolley was placed as close as possible to the pigs to keep the transmission distance similar to the distance of an on-body receiver. The distance varied from 62 cm (PigX) and 70 cm (PigY). 4 capsules were tested *in vivo* over two days.

1) In Vivo Trials: Static Power Procedure: The influence of different living tissues on the RSSI, PER and BER was investigated and potential temperature increase was monitored by the 4 on-board thermistors.

Before the first capsule was inserted, distance markers were placed at 2, 4, 6 and 8 cm from the stoma to allow for a more repeatable withdrawal rate. The tubing was marked with Kapton tape at the 60 cm mark in order to log the distance and return to approximately the same distance, when measurement was repeated. The capsule was inserted through the stoma 60 cm deep into the small bowel to keep it enclosed by as much body mass as possible providing a worst-case scenario where many different tissue layers surround the antenna system. To identify which types of tissues were present at the capsule location, the spot was initially scanned with transcutaneous ultrasound.

The capsule was then slowly withdrawn along the distance markers with a velocity of 2.7 mm/s. After the 8 cm mark was reached, the capsule remained stationary for 20 seconds. Subsequently the process was repeated twice. Time stamps were recorded to be able to relate the capsule location to the RF signal strength recordings. The experiment was performed with two capsules twice each and the temperature and RF data was continuously logged in excel files. The overall time period, for this part of the experiment, was approximately 45 minutes per pig.

2) In Vivo Trials: Variable Power Procedure: The next trial was conducted with the capsules operating at variable output power levels (0.1, 1, 4 and 10 mW or -10, 0, 6, 10 dBm) while fixed in position. One reason to perform this type of experiment was to gather data about thermal transfer under abnormal operating conditions where the pill is retained to test the possible temperature increase of tissue surrounding the antenna [43]. Another reason was to find the lowest transmission power that still allows for a wireless connection at a low error rate.

The same setup was used as in the previous experiments. The capsule was inserted through the stoma up to the 60 cm deep and the tubing was fixed in place with tape. The power levels increased stepwise with an off-period of 5 minutes between each increase. The pause served as recovery for the porcine tissue in case any temperature increase occurred during the signal transmission.

IV. RESULTS

A. Phantom Results

The capsules transmitting at a constant power level were placed inside the phantom, with the capsule orientated such that the tether connection pointed away from the RX, which was placed at a distance of 60 cm from the TX. Each capsule transmitted without interruption for 30 minutes. The recorded data showed a PER of 10^{-3} and BER of 10^{-5}, sufficient for a low error data transfer, with the signal strength ranging between -30 to -40 dBm. The PER test is used to examine the channel conditions during data transmission. All packets transmitted and received were error free and the BER was less than 10^{-3} as mentioned in [12], [44]. Kim *et al.* [45] state that the PER is used to quantify the data transmission efficiency and packet errors can be caused by either complete packet loss and/or bit errors. Failure in 10^{-3} of transmitted packets is therefore considered a satisfactory outcome. The variation in signal strength is thought to be due to manufacturing tolerances and detuning effects of the internal electrical components.

The same experimental setup was used with the capsules transmitting at a variable power level. Uninterrupted data were transmitted for one cycle, which lasted 37 minutes. The PER of these capsules varied between of 0 to 10^{-3} and the BER was recorded to be less than 10^{-5} for all power levels. The RSSI increased by 5 dBm from 0 to 0.1 mW, 3 dBm from 0.1 to 1 mW and 2 dBm from 1 to 10 mW.

A decrease of the RSSI of -2 dBm was observed when measuring the signal attenuation over distance and for every 10 cm introduced into the phantom, as shown in Fig. 8 (top). The average power of the capsules in the phantom at a distance of 60 cm between RX and TX was -31 dBm; this distance is comparable to the setup of the porcine trials. Fig. 8 (bottom) also shows the radiation distribution of the capsule antenna. A lower RSSI can be observed at the location of the tether and at 315° in the radiation pattern where the antenna is attached to the internal PCBs. No temperature increase is observed throughout the trials.

B. In Vivo Trial Results

1) In Vivo Results: Static Power Experiments: The first part of the experiments involved two RF capsules transmitting data at a single, constant power level while being gradually withdrawn from the small bowel. This experiment was used to gather data about PER, BER and the change of RSSI data under normal operating conditions in the small bowel.

The performance of the capsules varied in terms of signal strength, but overall the capsules showed a consistent output with a PER and BER of less than 10^{-5}, similar to the phantom tests. The RSSI showed a variation from -25 dBm to -56 dBm in the anaesthetized pigs at the first withdrawal step; this variation decreases from -28 dBm to -40 dBm towards the last withdrawal step, as indicated in Fig. 9. Most inserted capsules exhibit a RSSI below the detected RSSI of -31 dBm within the phantom.

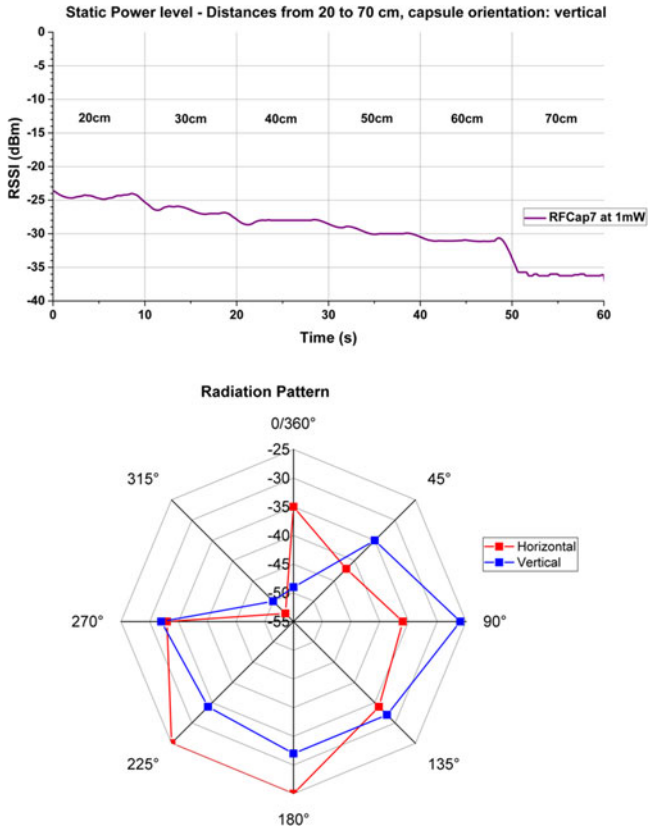

Fig. 8. Capsule immersed in phantom: Change of RSSI (dBm) over distance (top); radiation distribution in horizontal and vertical orientations (bottom).

The second run of each capsule insertion shows an offset compared to the first run as explained later, but approximately follows the same trend of the first insertion. During withdrawal, an increase and decrease of RSSI can be noticed, but during the fixed position the signal is mostly steady and the variation is reduced.

The small bowel of the euthanized PigX where the *in vivo* capsule trial took place was excised during a post-mortem gross visualization, as shown in Fig. 10. This section of tissue was inspected for presence of burns, inflammation and cuts and no evidence of tissue damage was observed.

2) In Vivo Results: Variable Power Experiments: The experiment was performed twice, each time with a different capsule. The temperature and RF data was continuously logged in Excel files during this trial. The duration of this experiment lasted approximately 80 mins per pig.

During this experiment, a PER and BER of less than 10^{-5} for every single power level was observed for each capsule. Fig. 9 illustrates the incremental increase of the RSSI when the power level was increased. The increase in power from the first (-10 dBm) to the second level (0 dBm) presents the biggest rise in power of 5 dBm. The step from 0 to 6 dBm generated a 2.5 dBm increase and from 6 to 10 dBm an increase of 1.5 dBm, which confirms the observation of the phantom test. The noisy signal at the start of some of the capsule insertions is due to concurrent activity on the laptop, which led to a variation in the power provided to the RX module.

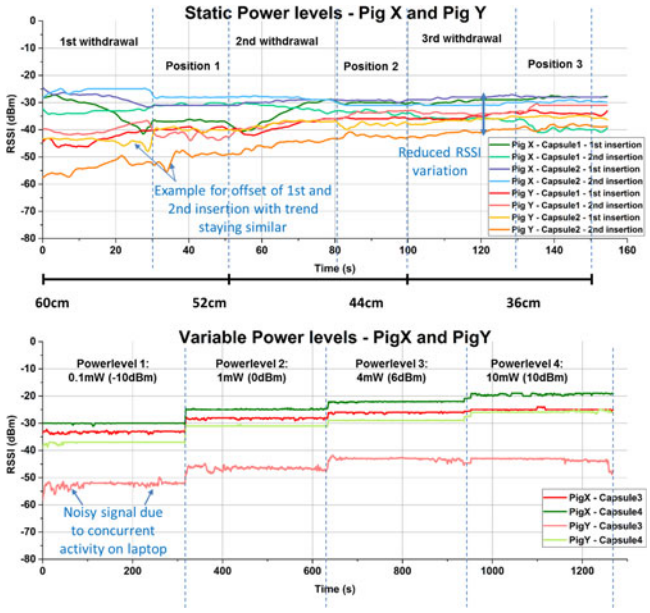

Fig. 9. RSSI comparison of all inserted capsules programmed with static power transmission (top) and increased power transmission (bottom) in pigs.

Fig. 10. Excised section of the small bowel that was in touch with the transmitting capsule.

Temperature rise of less than 1 °C was detected which conforms to the SAR standards [37], [38].

V. Discussion

A. Phantom Model

Compared to the almost omnidirectional pattern of the simulations the radiation pattern examined within the phantom shows a drop in power at the tether connection. This effect is due to the electric fields originating from the current running through the unshielded tether which are interfering with the fields of the capsule antenna. The simulation used a discrete port as feeding point together with the GND plane, as it was not possible to simulate the full system. Therefore, the radiation pattern originated from ideal conditions and the influence of the tether was not examined. This result demonstrates that the orientation of the capsule within the small bowel can affect the measured signal strength which can be seen in the variation of RSSI within the phantom of 20 dBm. Future applications will be completely

wireless and will not be affected by a tether, hence the measured radiation pattern will more likely represent the almost omnidirectional radiation of the simulated device. For the applications involving a tether an alternative data transmission mode with the data transmission cables in the tether can be used if necessary if there is any directional loss of data.

Concerning the change of signal strength over distance between the RX and TX, an attenuation of the signal with increasing distance was measured as expected; however the signal attenuation is negligible over a short distance of 10 cm.

B. In Vivo Model

1) In Vivo Results: Static Power Experiments: The capsules all vary with respect to signal strength, but all of them show a very low PER and BER at low power. This result strongly suggests that the concept of the conformal antenna offers a good alternative to internal antennas.

The results of the static power devices show that the variation in RSSI is the highest when the capsule is inserted to the furthest point (60 cm) from the stoma and is moved to the next stop. This effect is likely due to the increased insertion depth or increased tissue thickness and the variation in permittivity of the various tissues compared to the area nearer the stoma. Different dielectric properties of the capsule surrounding material lead to a shift in frequencies and change in power absorption and therefore cause a change of signal strength over the length of the withdrawal process. As the capsule nears the stoma there is a reduction in signal power variability observed in each capsule, which can be due to multiple factors such as increased dominance of a single tissue property, reduction in tissue mass surrounding the capsule as well as distance to the RX.

The change in capsule orientation, as previously observed in the phantom tests, together with the dielectric tissue property variation produce the largest detuning effects. The RSSI observed during the trials is also lower compared to the phantom tests, because more body mass is surrounding the antenna within the pig. The offset of each insertion, although the same capsule was used, is most likely due to the natural movement of the small bowel, which alters every insertion so that no insertion matches the previous one completely.

2) In Vivo Results: Variable Power Experiments: The increase in power levels confirms the impact of the transmission power of the TX on the transmitted signal strength. Good transmission performance is observed even at the lowest power of -10 dBm as shown by the low number of lost or faulty data packets.

No temperature increase was observed by the onboard thermistors over the full length of the investigation. This result confirms the SAR simulation result displayed in Fig. 11. The highest SAR value of 0.08 W/kg is well below the FCC recommended limit of 1.6 W/kg for 10 grams of tissue mass with an antenna excitation power of 0.5 W. The highest power (10 mW) used is still well below maximum power allowed in terms of SAR restrictions.

The placement distance between the RX and PigX stoma is extended by 8 cm for PigY which, according to the phantom tests, would cause a signal attenuation of approximately −2 dBm and can therefore be neglected.

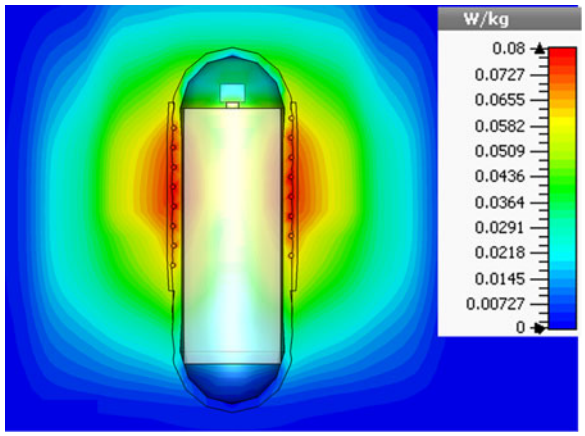

Fig. 11. SAR distribution of the simulated antenna system.

The lack of localized tissue heating in conjunction with low power transmission shows that conformal antennas is a viable technology for ingestible and short term implantable medical devices, such as capsule endoscopes.

VI. Conclusion

All capsules demonstrated a satisfactory performance at a data rate of 256 kbps in *in vivo* and phantom experiments. Data transmission was achieved with low error rates ($<10^{-3}$) and a temperature increase of less than 1 °C was detected for the tissue surrounding the antenna.

RSSI as low as −58 dBm with low TX output power levels of −10 dBm still offer a low PER and BER irrespective of the location of the capsule within the small bowel. The CC1110 receiver exhibits a sensitivity of −95 dBm, which provides us with a wider margin for varying operation conditions.

The signal strength of the inserted capsules varies with distance and orientation to the receiver and with tissue surrounding the capsules as well as insertion depth.

The polarisation of the transmitting antenna should ideally be circular. The designed antenna displays an elliptical polarisation with major axis of polarisation in the horizontal direction, using Kraus' approach [46]. The potential mismatch is however offset by the circular polarisation of the receiver, as well as the almost omnidirectional radiation of the transmitter. However, the data transmission results show that this mismatch is overcome reasonably.

The *in vivo* results successfully demonstrate the concept of placing a conformal antenna on the outside of an ingestible capsule and the ability of transmitting data wirelessly from an ingestible medical device from within a patient's body, without causing harmful temperature effects to the human body tissue.

Acknowledgment

The authors would like to thank the team from the National Physical Laboratory (NPL), especially Mr. Ralf Mouthaan.

REFERENCES

[1] N. Kurniawan and M. Keuchel, "Technology," in *Video Capsule Endoscopy: A Reference Guide and Atlas*, M. Keuchel, F. Hagenmüller, and H. Tajiri, Eds. Berlin, Germany: Springer, 2014, pp. 15–20.

[2] G. Iddan, G. Meron, A. Glukhovsky, and P. Swain, "Wireless capsule endoscopy," *Nature*, vol. 405, no. 6785, pp. 417–417, 2000.

[3] V. K. Sharma, "The future is wireless: Advances in wireless diagnostic and therapeutic technologies in gastroenterology," *Gastroenterology*, vol. 137, no. 2, pp. 434–439, Aug. 2009.

[4] A. Koulaouzidis, D. K. Iakovidis, A. Karargyris, and E. Rondonotti, "Wireless endoscopy in 2020: Will it still be a capsule?" *World J. Gastroenterol.*, vol. 21, no. 17, pp. 5119–5130, 2015.

[5] Sonopill, Sonopill—Future of Capsule Endoscopy. 2016. [Online]. Available: http://sonopill.dundee.ac.uk/

[6] J. L. Toennies, G. Tortora, M. Simi, P. Valdastri, and R. J. Webster, "Swallowable medical devices for diagnosis and surgery: The state of the art," *Proc. Inst. Mech. Eng. C—J. Mech. Eng. Sci.*, vol. 224, no. C7, pp. 1397–1414, 2010.

[7] L. Sang Heun *et al.*, "A wideband spiral antenna for ingestible capsule endoscope systems: Experimental results in a human phantom and a pig," *IEEE Trans. Biomed. Eng.*, vol. 58, no. 6, pp. 1734–1741, Jun. 2011.

[8] R. Alrawashdeh, Y. Huang, P. Cao, and E. Lim, "A new small conformal antenna for capsule endoscopy," in *Proc. 7th Proc. Eur. Conf. Antennas Propag.*, 2013, pp. 220–223.

[9] Y. Sumin, K. Kihyun, and N. Sangwook, "Outer-wall loop antenna for ultrawideband capsule endoscope system," *IEEE Antennas Wireless Propag. Lett.*, vol. 9, pp. 1135–1138, 2010.

[10] C. Liu, Y. X. Guo, and S. Xiao, "Circularly polarized helical antenna for ISM-band ingestible capsule endoscope systems," *IEEE Trans. Antennas Propag.*, vol. 62, no. 12, pp. 6027–6039, Dec. 2014.

[11] M. Je *et al.*, "Wireless sensor microsystems for emerging biomedical applications (Invited)," in *Proc. IEEE Int. Symp. Radio-Freq. Integr. Technol.*, 2015, pp. 139–141.

[12] R. Das and H. Yoo, "A wideband circularly polarized conformal endoscopic antenna system for high-speed data transfer," *IEEE Trans. Antennas Propag.*, vol. 65, no. 6, pp. 2816–2826, Jun. 2017.

[13] P. M. Izdebski, H. Rajagopalan, and Y. Rahmat-Samii, "Conformal ingestible capsule antenna: A novel chandelier meandered design," *IEEE Trans. Antennas Propag.*, vol. 57, no. 4, pp. 900–909, Apr. 2009.

[14] F. Merli, B. Fuchs, and A. K. Skrivervik, "Influence of insulation for implanted antennas," in *Proc. 3rd Eur. Conf. Antennas Propag.*, 2009, pp. 196–199.

[15] A. K. Skrivervik, "Implantable antennas: The challenge of efficiency," in *Proc. 7th Eur. Conf. Antennas Propag.*, 2013, pp. 3627–3631.

[16] A. Kiourti and K. Nikita, "Implantable antennas: A tutorial on design, fabrication, and in vitro/in vivo testing," *IEEE Microw. Mag.*, vol. 15, no. 4, pp. 77–91, Jun. 2014.

[17] P. Valdastri, A. Menciassi, A. Arena, C. Caccamo, and P. Dario, "An implantable telemetry platform system for in vivo monitoring of physiological parameters," *IEEE Trans. Inf. Technol. Biomed.*, vol. 8, no. 3, pp. 271–278, Sep. 2004.

[18] M. R. Basar *et al.*, "The use of a human body model to determine the variation of path losses in the human body channel in wireless capsule endoscopy," *Prog. Electromagn. Res.*, vol. 133, pp. 495–513, 2013.

[19] A. Vander Vorst, A. Rosen, and Y. Kotsuka, *RF/Microwave Interaction with Biological Tissues*. Hoboken, NJ, USA: Wiley, 2006.

[20] C. Gabriel, S. Gabriel, and E. Corthout, "The dielectric properties of biological tissues: I. Literature survey," *Phys. Med. Biol.*, vol. 41, no. 11, pp. 2231–49, Nov. 1996.

[21] S. Gabriel, R. W. Lau, and C. Gabriel, "The dielectric properties of biological tissues: II. Measurements in the frequency range 10 Hz to 20 GHz," *Phys. Med. Biol.*, vol. 41, no. 11, pp. 2251–2269, Nov. 1996.

[22] S. Gabriel, R. W. Lau, and C. Gabriel, "The dielectric properties of biological tissues: III. Parametric models for the dielectric spectrum of tissues," *Phys. Med. Biol.*, vol. 41, no. 11, pp. 2271–2293, Nov. 1996.

[23] T. Chrysikos, I. Zisi, and S. Kotsopoulos, "Channel modeling and path loss characterization for in-body propagation at MICS and ISM bands," in *Proc. Wireless Telecommun. Symp.*, 2016, pp. 1–7.

[24] A. Menciassi, G. Ciuti, and C. Cavallotti, "Future developments of video capsule endoscopy: Hardware," in *Video Capsule Endoscopy: A Reference Guide and Atlas*, M. Keuchel, F. Hagenmüller, and H. Tajiri, Eds. Berlin, Germany: Springer, 2014, pp. 543–556.

[25] Z. Li *et al.*, "The current main types of capsule endoscopy," in *Handbook of Capsule Endoscopy*, Z. Li, Z. Liao, and M. McAlindon, Eds. Dordrecht, The Netherlands: Springer, 2014, pp. 5–45.

[26] T. S. Kim, S. Y. Song, H. Jung, J. Kim, and E. S. Yoon, "Micro capsule endoscope for gastro intestinal tract," in *Proc. 29th IEEE Eng. Med. Biol. Soc. Annu. Int. Conf.*, 2007, pp. 2823–2826.

[27] J. Thoné, S. Radiom, D. Turgis, R. Carta, G. Gielen, and R. Puers, "Design of a 2 Mbps FSK near-field transmitter for wireless capsule endoscopy," *Sens. Actuators A, Phys.*, vol. 156, no. 1, pp. 43–48, Nov. 2009.

[28] A. Wang *et al.*, "Wireless capsule endoscopy," *Gastrointestinal Endoscopy*, vol. 78, no. 6, pp. 805–815, Dec. 2013.

[29] B. A. Whitmer, M. Raphael, and B. Warren, "Video capsule endoscopy: The past, present, and future," *J. Gastrointestinal Digestive Syst.*, vol. 1, p. 001, 2011.

[30] D. Bandorski *et al.*, "Contraindications for video capsule endoscopy," *World J. Gastroenterol.*, vol. 22, no. 45, pp. 9898–9908, 2016.

[31] J. Faerber, G. Cummins, and M. P. Y. Desmulliez, "Design of conformal wideband antennas for capsule endoscopy within a body tissue environment," in *Proc. 46th Eur. Microw. Conf.*, 2016, pp. 1223–1226.

[32] A. Kiourti and K. S. Nikita, "A review of in-body biotelemetry devices: Implantables, ingestibles, and injectables," *IEEE Trans. Biomed. Eng.*, vol. 64, no. 7, pp. 1422–1430, Jul. 2017.

[33] T. Castel *et al.*, "Improved reception of in-body signals by means of a wearable multi-antenna system," *Int. J. Antennas Propag.*, vol. 2013, 2013, Art. no. 328375.

[34] X. Cheng, J. Wu, R. Blank, D. E. Senior, and Y. K. Yoon, "An Omnidirectional wrappable compact patch antenna for wireless endoscope applications," *IEEE Antennas Wireless Propag. Lett.*, vol. 11, pp. 1667–1670, 2012.

[35] F. Merli, L. Bolomey, J. Zurcher, G. Corradini, E. Meurville, and A. K. Skriverviky, "Design, realization and measurements of a miniature antenna for implantable wireless communication systems," *IEEE Trans. Antennas Propag.*, vol. 59, no. 10, pp. 3544–3555, Oct. 2011.

[36] X. Lisheng, M. Q. H. Meng, C. Yawen, H. Chao, and W. Haibin, "Influence of animal body on ingested wireless device before and after death," in *Proc. IEEE/ASME Int. Conf. Adv. Intell. Mechatronics*, 2008, pp. 176–181.

[37] *IEEE Standard for Safety Levels with Respect to Human Exposure to Radio Frequency Electromagnetic Fields, 3 kHz to 300 GHz*, IEEE Standard C95.1-2005 (Revision of IEEE Standard C95.1-1991), 2006, pp. 1–238.

[38] M. Beccani, E. Susilo, C. Di Natali, and P. Valdastri, "SMAC—A modular open source architecture for medical capsule robots," *Int. J. Adv. Robot. Syst.*, vol. 11, Nov. 2014, Art. no. 188.

[39] F. Merli, B. Fuchs, J. R. Mosig, and A. K. Skrivervik, "The effect of insulating layers on the performance of implanted antennas," *IEEE Trans. Antennas Propag.*, vol. 59, no. 1, pp. 21–31, Jan. 2011.

[40] M. R. Yuce and T. Dissanayake, "Easy-to-swallow antenna and propagation," *IEEE Microw. Mag.*, vol. 14, no. 4, pp. 74–82, Jun. 2013.

[41] R. Jegadeesan, G. Yong Xin, and J. Minkyu, "Electric near-field coupling for wireless power transfer in biomedical applications," in *Proc. IEEE MTT-S Int. Microw. Workshop Ser. RF Wireless Technol. Biomed. Healthcare Appl.*, 2013, pp. 1–3.

[42] A. P. Gregory and R. N. Clarke, "Dielectric metrology with coaxial sensors," *Meas. Sci. Technol.*, vol. 18, no. 5, 2007, Art. no. 1372.

[43] M. Rezapour, C. Amadi, and L. B. Gerson, "Retention associated with video capsule endoscopy: Systematic review and meta-analysis," *Gastrointestinal Endoscopy*, vol. 85, no. 6, pp. 1157–1168, Jun. 2017.

[44] W. Lei *et al.*, "A programmable microsystem using system-on-chip for real-time biotelemetry," *IEEE Trans. Biomed. Eng.*, vol. 52, no. 7, pp. 1251–1260, Jul. 2005.

[45] S. Kim *et al.*, "Evaluation of a 433 MHz band body sensor network for biomedical applications," *Sensors (Basel)*, vol. 13, no. 1, pp. 898–917, Jan. 14, 2013.

[46] J. D. Kraus, "The helical antenna," *Proc. IRE*, vol. 37, no. 3, pp. 263–272, 1949.

Julia Faerber (S'14) received the B.Sc. degree in microsystem engineering from the University of Gelsenkirchen, Gelsenkirchen, Germany, in 2008, and the M.Sc. degree in biomedical engineering from the University of Dundee, Dundee, U.K., in 2010. She is currently working toward the Ph.D. degree in antenna design with Heriot-Watt University, Edinburgh, U.K.

Gerard Cummins (M'03) received the B.Eng. degree in microelectronic and electronic engineering from University College Cork, Cork, Ireland, and the Ph.D. degree in engineering from the University of Edinburgh, Edinburgh, U.K., in 2011. He is currently a Research Associate with Heriot-Watt University, Edinburgh.

Sumanth Kumar Pavuluri received the Ph.D. degree from Heriot-Watt University, Edinburgh, U.K., in 2011. He is currently a Postdoctoral Research Associate with Heriot-Watt University working on microwave sensing, micromachined antennas, and microwave applicators for curing and heating applications.

Paul Record, photograph and biography not available at the time of publication.

Adrian R. Ayastuy Rodriguez, photograph and biography not available at the time of publication.

Holly S. Lay received the Bachelor of Science degree in electrical engineering and the Ph.D. degree in engineering physics in 2011, both from Queen's University, Kingston, ON, Canada. She is currently a Research Associate with the University of Glasgow, Glasgow, U.K.

Rachael McPhillips, photograph and biography not available at the time of publication.

Benjamin F. Cox completed the B.Sc. degree in biology from Dalhousie University, Halifax, NS, Canada. He completed his medical studies at the First Faculty of Medicine, Charles University, Prague, Czech Republic, in 2010. He is currently involved in the Sonopill program as the Clinical Research Fellow. In addition, he is enrolled in a Ph.D. program aimed at characterizing gastrointestinal pathology with capsule-based multimodal imaging.

Ciaran Connor, photograph and biography not available at the time of publication.

Rachael Gregson graduated from the Royal (Dick) School of Veterinary Studies, Midlothian, U.K., in 2003, and worked in mixed private practice before returning to Edinburgh to complete a Residency in veterinary anesthesia, where she developed a keen interest in pig anesthesia. She has been an Anesthetist in the Wellcome Trust Critical Care Laboratory for Large Animals, Roslin Institute, Midlothian, U.K., since 2016.

Richard Eddie Clutton received the B.V.Sc. degree from the University of Liverpool, Liverpool, U.K., in 1981, and the Diploma of the European College of Veterinary Anaesthesia in 1996. He is the Head of veterinary anesthesia with the Royal (Dick) School of Veterinary Studies and the Director of the Wellcome Trust Critical Care Laboratory for Large Animals, Roslin Institute, Midlothian, U.K.

Sadeque Reza Khan received the B.Sc. degree in electronics and telecommunication engineering from the University of Liberal Arts Bangladesh, Dhaka, Bangladesh, and the M.Tech. degree in very large scale integration design from the National Institute of Technology Karnataka, Mangalore, India. He is currently working toward the Ph.D. degree in electrical engineering with Heriot-Watt University, Edinburgh, U.K.

Sandy Cochran, photograph and biography not available at the time of publication.

Marc P. Y. Desmulliez (SM'87) received the Ph.D. degree in optoelectronics from Heriot-Watt University, Edinburgh, U.K., in 1995. He is currently a Professor of microsystems engineering with Heriot-Watt University and leads the Multimodal Sensing and Micromanipulation Research Group.